

NIST GCR 03-855

An Analysis of Effective Thermal Properties of Thermally Thick Materials

Frederick W. Mowrer
Department of Fire Protection Engineering
University of Maryland
College Park, MD 20742-3031

NIST

National Institute of Standards and Technology
Technology Administration, U.S. Department of Commerce

NIST GCR 03-855

An Analysis of Effective Thermal Properties of Thermally Thick Materials

Prepared for
*U.S. Department of Commerce
Building and Fire Research Laboratory
National Institute of Standards and Technology
Gaithersburg, MD 20899-8661*

By
Frederick W. Mowrer
Department of Fire Protection Engineering
University of Maryland
College Park, MD 20742-3031

July 2003



U.S. Department of Commerce
Donald L. Evans, Secretary

Technology Administration
Phillip J. Bond, Under Secretary for Technology

National Institute of Standards and Technology
Arden L. Bement, Jr., Director

Notice

This report was prepared for the Building and Fire Research Laboratory of the National Institute of Standards and Technology under Grant number 60NANB2D0123. The statement and conclusions contained in this report are those of the authors and do not necessarily reflect the views of the National Institute of Standards and Technology or the Building and Fire Research Laboratory.

An analysis of effective thermal properties of thermally thick materials

Frederick W. Mowrer, Ph.D., P.E., FSFPE
Department of Fire Protection Engineering
University of Maryland

Abstract

The standard methods used to derive effective thermal properties of thermally thick materials based on bench-scale radiant exposure tests are reviewed and analyzed. These methods are compared with numerical calculations for the same boundary conditions. These comparisons show that the standard analytical methods for predicting surface temperature histories are not accurate because they either ignore heat losses from the surface or do not adequately treat the highly nonlinear reradiative surface heat loss term. A method is presented for determining more accurate values for the thermal inertia based on effective values for this term published widely in the literature. It is found that actual thermal inertias tend to be lower by about a factor of 1.3 to 2.7 when compared with reported effective values for a wide range of conditions. This can have a significant effect on flame spread predictions for models that rely on accurate values for the thermal inertia.

Keywords: Ignition, thermal inertia, thermally thick materials

Nomenclature

c	specific heat (kJ/kg.K)
h	heat transfer coefficient (kW/m ² .K)
k	thermal conductivity (kW/m.K)
\dot{q}''	heat flux (kW/m ²)
t	time (s)
α	absorptivity (-)
ε	emissivity (-)
ΔT	temperature rise above ambient (K)
ρ	density (kg/m ³)
σ	Stefan-Boltzmann constant (5.67×10^{-11} kW/m ² .K ⁴)

subscripts

act	actual
c	characteristic, convective
cr	critical
eff	effective
i	incident
ig	ignition

<i>max</i>	maximum
<i>o</i>	ambient
<i>r</i>	radiative
<i>s</i>	surface
<i>t</i>	total

Introduction

In order to assess the ignition and flame spread characteristics of solid materials, it is necessary to know their thermal properties. For thermally thick solids, it is well known [1, 2] that the thermal inertia of the material governs the rate of rise of the surface temperature and consequently the time to ignition. The thermal inertia, $k\rho c$, is the product of the thermal conductivity, k , the density, ρ , and the specific heat, c , of the material. These properties can vary over the temperature range of interest for flammability evaluation, but for engineering purposes the thermal inertia is usually treated as a constant effective property.

Determination of the effective thermal inertia of a material is typically based on evaluation of results from small-scale radiant exposure test methods, including the LIFT apparatus [3], the Cone Calorimeter [4] and the FM Fire Propagation Apparatus [5]. In these test methods, small test specimens are exposed to a range of constant incident radiant heat fluxes and the time to ignition is measured. Based on these results, the application of heat transfer theory and a number of assumptions, effective thermal properties are determined. The assumptions that are made can have a strong influence on the effective thermal properties that are derived.

Steinhaus [6] showed experimentally that the value of $k\rho c$ for PMMA evaluated using the LIFT methodology [3] was over-predicted by a factor of more than four when compared to the product of all three properties evaluated individually from the reported temperature-dependent material properties. Later, Cordova, et al., [7] compared these values with the analytical model of Long, et al., [8] and demonstrated several factors that have a significant effect on the ultimate evaluation of the thermal properties. In these previous studies, the authors concentrated on the phenomenological aspects of the problem and do not present potential adjustments to the methodology used to evaluate the effective thermal properties.

In this paper, the traditional methods for evaluating the effective thermal properties of thermally thick materials are reviewed and compared with numerical calculations. Based on these comparisons, a method is presented for adjusting effective thermal inertias to more accurately represent the actual thermal inertias of materials. The analysis presented here is based only on thermal arguments and does not address additional issues related to the determination of material flammability properties. These issues are associated with the generation of sufficient fuel for sustained ignition, in-depth generation of fuel, pilot location, and other factors [1]. Similar analyses to those presented here should be performed to address the impact of these physical and chemical processes on the determination of material flammability properties.

Theoretical analysis

Consider a thermally thick solid with a planar surface subjected to a constant and uniform incident heat flux, $\alpha\dot{q}_i''$, with convective and reradiative cooling at the surface. Assume that the surface cooling can be represented in terms of a constant heat transfer coefficient, h . This scenario is represented in Figure 1. The analytical solution [8] for this scenario can be expressed nondimensionally as:

$$\frac{\Delta T_s}{\Delta T_c} = 1 - \exp\left(-\frac{t}{t_c}\right) \cdot \operatorname{erfc}\left(\sqrt{\frac{t}{t_c}}\right) \quad (1)$$

where $\Delta T_c \equiv \frac{\alpha\dot{q}_i''}{h_t}$ and $t_c \equiv \frac{k\rho c}{h_t^2}$.

The characteristic temperature rise, ΔT_c , represents the maximum temperature rise that would occur if the surface were perfectly insulated, while the characteristic time, t_c , represents the ratio between the conduction of heat into the surface and the convection and reradiation of heat from the surface. Materials with low thermal inertias are relatively poor conductors, with the implication that they will “trap” heat at the surface, causing the surface temperature to increase more quickly than for materials with higher thermal inertias.

Equation 1 is based on a constant total surface heat transfer coefficient, which is inaccurate. This coefficient represents both convective and reradiative cooling of the surface:

$$h_t(T_s - T_o) = h_c(T_s - T_o) + \varepsilon\sigma(T_s^4 - T_o^4) \equiv h_c(T_s - T_o) + h_r(T_s - T_o) \quad (2)$$

In the small-scale test devices generally used to evaluate effective material properties, the convective heat transfer coefficient, h_c , approaches a relatively constant value fairly quickly, but the reradiative coefficient, h_r , varies with the third power of the absolute surface temperature, so it continues to increase significantly as the surface temperature increases. This nonlinearity makes difficult the evaluation of effective thermal properties by approximate means.

The maximum theoretical value for the total heat transfer coefficient, $h_{t,max}$, can be evaluated based on the characteristic absolute surface temperature, T_c , by evaluating the energy balance at the surface under conditions where in-depth conduction is neglected:

$$\alpha\dot{q}_i'' = h_c(T_c - T_o) + \varepsilon\sigma(T_c^4 - T_o^4) \equiv h_{t,max}(T_c - T_o) \quad (3)$$

From Equation 3 the characteristic temperature is calculated as a function of the incident heat flux. Once the characteristic temperature rise is determined by solving the surface energy balance, the maximum total heat transfer coefficient can be calculated directly. The solution for Equation 3 is illustrated in Figure 2 for a range of incident heat fluxes, based on a surface with perfect emissivity ($\varepsilon = 1$), a constant convective heat transfer coefficient with a value of $h_c = 15$

W/m².K, and an ambient temperature of 20°C (293K). In reality, the convective heat transfer coefficient is expected to vary with the 1/4th power of the surface temperature rise [2], so this effect is relatively small and is neglected for the present analysis.

The value for the maximum total heat transfer coefficient determined from Equation 3 can be used to evaluate a characteristic time, $t_{c,max} = k\rho c / h_{t,max}$, but it should be recognized that use of this value in Equation 1 will not yield an accurate solution for the surface temperature rise. This is because this value for the characteristic time will cause surface losses to be overestimated, by a very large margin during the early stage of surface heating and diminishing with time as the surface temperature approaches the characteristic value. When evaluating ignition delay times, this error will translate to an over-prediction of the ignition delay time. The higher the incident heat flux, the smaller the expected error will be. Nonetheless, this value for the characteristic time is fixed based on the incident heat flux and will yield the correct asymptotic value for the surface temperature rise, so it is used for normalizing and comparing data.

Two similar alternative approaches have been widely used to determine effective thermal properties [1, 9, 10] from small-scale tests. The most widely used approach has been to use the short time limit solution based on the Laplace transform of Equation 1 [8], which can be expressed in nondimensional terms as:

$$\frac{\Delta T_s}{\Delta T_c} = \sqrt{\frac{4 t}{\pi t_c}} \quad (4)$$

where ΔT_c and t_c are as previously defined. This solution represents the limit case of no convective or radiative heat losses from the surface, i.e., the constant heat flux solution. It is referred to as the “no-loss” solution in this paper. This solution is accurate only for very short times, with $t/t_c \sim O(0.01)$ or less, when compared with Equation 1. Physically, this is because surface heat losses rapidly become significant as the surface temperature increases under the imposed heat flux. Ignition delay times will therefore be under-predicted by Equation 4, with larger discrepancies found at the lowest heat fluxes. From a practical standpoint, ignition data is not collected for the very high heat fluxes that would be associated with this time scale and, consequently, consideration of surface losses is important for thermal property determination.

The second widely used approach [10] is similar to the first, but instead of ignoring convective and radiative heat losses from the surface, this approach assumes that these surface losses remain constant at a value equal to the critical incident heat flux required to ignite the material, \dot{q}_{cr}'' . In nondimensional terms, this solution, referred to here as the “Tewarson” solution, can be expressed as:

$$\frac{\Delta T_s}{\Delta T_c} = \left(1 - \frac{\dot{q}_{cr}''}{\alpha \dot{q}_i''} \right) \sqrt{\frac{4 t}{\pi t_c}} \quad (5)$$

At high incident heat fluxes, this solution converges to the solution represented by Equation 4 because the ratio between the critical heat flux and the incident heat flux goes to zero. At a heat

flux ratio of one, Equation 5 would suggest no temperature rise at the surface, a clearly incorrect result because at this heat flux the surface temperature should become the ignition temperature by definition. In essence, the term in parentheses in Equation 5 serves as a constant adjustment factor to reduce the net heat flux to the surface for the no loss solution represented by Equation 4, with the consequence that different effective thermal properties are determined based on this factor. The adjustment factor represented in Equation 5 implicitly assumes that surface losses at the critical heat flux condition are representative of surface losses over the entire heating process. This constant adjustment factor overestimates such losses at short times and consequently overestimates ignition delay times, with the effects being more evident at lower incident heat fluxes. An alternative adjustment factor is described below, based on the numerical results described next.

Numerical analysis

The analytical solutions represented by Equations 1, 4 and 5 were compared with numerical results for a range of incident heat fluxes and material thermal properties. The numerical results were calculated using an explicit finite difference scheme on a spreadsheet. A convective-radiative boundary condition was specified at the exposed face, while an insulated boundary condition was used at the back face. The backface temperature rise was checked to assure that it was less than 5 percent of the front face temperature rise, consistent with the thermally thick assumption for the analytical solutions. A surface absorptivity and emissivity of unity, a constant convective heat transfer coefficient of $h_c = 15 \text{ W/m}^2\cdot\text{K}$ and an ambient temperature of 20°C (293K) were used for both the analytical and the numerical calculations where these terms were needed.

Comparisons were performed for incident heat fluxes of 25, 50, 75 and 100 kW/m^2 , and for thermal inertias of 0.001, 0.1 and $1.0 \text{ (kW/m}^2\cdot\text{K)}^2\cdot\text{s}$. The specific thermal properties used for the calculations and comparisons are provided in Table 1. The low-end of the thermal inertia range is representative of the order of magnitude for low density insulating materials, while the high end is representative of relatively high-density building materials such as concrete. The middle value is representative of the order of magnitude for many typical building materials such as gypsum wallboard and wood products. An ignition temperature of 350°C was assumed for all materials. This ignition temperature is associated with a critical heat flux of 13.1 kW/m^2 in accordance with Equation 3.

Table 1. Thermal properties of materials used for numerical analysis.

Qualitative thermal inertia	Conductivity, k (kW/m.K)	Density, ρ (kg/m ³)	Spec. heat, c (kJ/kg.K)	$k\rho c$ (kW/m ² .K) ² .s	Ignition temperature (°C)
Low	.00005	20	1.0	0.001	350
Medium	.00012	600	1.4	0.1	350
High	.000625	2000	0.8	1.0	350

Values for the characteristic temperature rise and characteristic time for the conditions evaluated numerically are provided in Table 2. Results of the calculations are shown in Figures 3(a)-(d) for the four incident heat fluxes evaluated, with the horizontal dashed lines indicating the ignition temperature rise and the vertical arrows showing the different ignition times predicted by the different methods. Comparisons of the predicted times to ignition based on the exact solution (Equation 1), the no loss solution (Equation 4), the Tewarson solution (Equation 5) and the numerical calculations for the low, medium and high thermal inertia materials are provided in Table 3. The numerical results all converge to the same values for all three thermal inertias at the same incident heat fluxes when expressed in terms of the ΔT_c and $t_{c,max}$ defined above.

Table 2. Characteristic temperatures, total heat transfer coefficients and characteristic times for the range of scenarios analyzed.

			Thermal inertia (kW/m ² .K) ² .s		
			0.001	0.1	1.0
Incident heat flux (kW/m ²)	ΔT_c (°C)	$h_{t,max}$ (W/m ² .K)	Characteristic time (s)		
25	462.6	54	0.342	34.24	342.4
50	629.0	79	0.158	15.83	158.3
75	739.1	101	0.097	9.71	97.1
100	823.4	121	0.068	6.78	67.8

Table 3. Predicted times to ignition for low thermal inertia material at different heat fluxes based on an assumed ignition temperature of 350°C.

Incident heat flux (kW/m ²)		Dimensionless ignition times (t/t _c)					
		Analytical solutions			Numerical results		
		Exact	No loss	Tewarson	Low thermal inertia	Medium thermal inertia	High thermal inertia
25	0.713	3.02	0.40	1.76	1.20	1.20	1.20
50	0.525	0.71	0.22	0.40	0.34	0.34	0.34
75	0.447	0.40	0.16	0.23	0.21	0.21	0.21
100	0.401	0.29	0.13	0.17	0.16	0.16	0.16

Discussion

The comparison of analytical solutions with numerical calculations demonstrates that none of the analytical solutions accurately captures the surface temperature history of a thermally thick solid exposed to a constant incident heat flux and subject to convective and reradiative losses from the surface. The assumption of no losses from the surface becomes increasingly incorrect as the

surface temperature increases. The nonlinearity of the surface reradiation term also limits the use of simple analytical solutions for the accurate representation of thermal property data. While such simple solutions are useful for comparison purposes and for simple ignition and flame spread models based on the same assumptions, they do not accurately portray thermal properties for models based on more accurate boundary conditions.

The numerical results demonstrate that the actual surface temperature rise falls somewhere between the exact solution based on a maximum heat transfer coefficient (Equation 1) and the no loss, or constant heat flux, solution (Equation 4). As shown in Figures 3(a)-(d), this is true for all the cases evaluated here and would be expected to be true in general. Both of the analytical solutions and the numerical results are virtually the same at very short times, before the surface temperature has increased significantly. This is to be expected because heat losses are relatively small. As the surface temperature continues to increase, the different solutions diverge from each other because of their different treatments of the surface losses.

It was found that selection of grid size was important in capturing the early surface temperature rise accurately in the numerical calculations. Grids that were too large would result in slower initial increases in surface temperature because the surface node would represent a greater volume of material to absorb the incident heat. This was only important for capturing the surface temperature rise at very short times. Comparison of calculated surface temperature with analytical results at short times was used to determine if sufficient grid resolution was used. When the numerical results closely matched the analytical solutions at very early times, it was apparent that sufficient resolution had been achieved.

A number of different time steps were initially used. If a selected time step was too large, the explicit solution would become unstable as evidenced by wild fluctuations in temperatures. Eventually, time steps of 0.01 and 0.001 times the maximum characteristic temperature were attempted. The lower value always produced stable results for the grid sizes used, so it was used for most of the calculations.

In general, it was found that the Tewarson solution (Equation 5) yielded the most accurate estimates of ignition time for the three analytical solutions evaluated, with the exception of the 25 kW/m² incident heat flux case. This is evident in Table 3 as well as in Figures 3(a)-(d). To some extent, this is coincidental because Figures 3(a)-(d) clearly show that the Tewarson solution is not accurately tracking the surface temperature history, even though it is intersecting the real surface temperature at a time nearest the ignition time for the higher heat flux cases. Since the Tewarson solution depends on the critical heat flux for ignition, which in turn depends on the ignition temperature, general conclusions cannot be drawn from the limited comparisons performed here, other than that the Tewarson solution does not perform well as the incident heat flux approaches the critical heat flux.

The effective thermal properties of materials determined by the current methods of analyzing ignition data from small-scale radiant exposure tests can still be used in models or formulae based on similar assumptions regarding boundary conditions, but these effective properties are not suitable for use with models based on different boundary conditions. In particular, many CFD models, such as FDS [11], that predict flame spread on surfaces explicitly account for

convective and reradiative losses from the surface; for these models, the actual thermal properties are needed rather than the effective properties reported extensively in the literature.

Determination of new adjustment factor

There is a large body of effective thermal property data that has been generated based on application of Equation 4 or Equation 5 to experimental data. A method to adjust this existing data to more accurately represent the actual thermal properties for use with models that need these actual properties would be desirable. One method for doing this is described here. This method can also be used for the analysis of ignition data acquired in the future.

In essence, what is needed is an adjustment factor that will force the no-loss analytical solution (Equation 4) through the ignition point. This concept is illustrated in Figure 4. Note the similarity with the Tewarson solution (Equation 5), which includes a similar adjustment factor. As illustrated in Figure 4, the adjustment factor that is needed is simply the ratio of the numerical surface temperature rise to the no-loss surface temperature rise at the time of ignition, The equation representing this new curve can be expressed as:

$$\frac{\Delta T_{ig}}{\Delta T_c} = \left[\frac{(\Delta T_s / \Delta T_c)_{numerical}}{(\Delta T_s / \Delta T_c)_{no-loss}} \right] \cdot \sqrt{\frac{4 t_{ig}}{\pi t_{c,act}}} = \sqrt{\frac{4 t_{ig}}{\pi t_{c,eff}}} \quad (6)$$

The second part of Equation 6 indicates that this solution is also the solution for the no-loss solution for the case of a time constant based on the effective thermal inertia. Since the time constants are directly proportional to the thermal inertias by definition, the ratios between the thermal inertias can be expressed as:

$$\frac{(k\rho c)_{act}}{(k\rho c)_{eff}} = \frac{t_{c,act}}{t_{c,eff}} = \left[\frac{(\Delta T_s / \Delta T_c)_{numerical}}{(\Delta T_s / \Delta T_c)_{no-loss}} \right]_{@t=t_{ig}}^2 \quad (7)$$

The temperature ratios in Equation 7 are tabulated in Table 4 as a function of the dimensionless time for the range of heat fluxes considered here. The temperature ratios tabulate in Table 4 are also illustrated in Figure 5, which shows how similar the numerical solutions are for different incident heat fluxes when plotted nondimensionally.

The ratio between the numerical surface temperature rise and the no-loss temperature rise, referred to as the “surface temperature ratio,” is shown in Table 5 and in Figure 6 along with the ratio between the actual and effective thermal inertias, which is called the “thermal inertia ratio.” The thermal inertia ratio is calculated on the basis of Equation 7. Table 5 and Figure 6 are of more practical use than Table 4 for calculating actual thermal inertias from effective thermal inertias. A more extensive tabulation based on a time increment of 0.001 t_c has been developed, but is too large for inclusion here. Table 5 could also be expanded to include more intermediate heat fluxes in order to reduce the amount of interpolation need to use it. The use of Table 5 is demonstrated by example below.

Table 4. Dimensionless surface temperatures as a function of dimensionless times based on Equation 4 and the numerical results for the range of incident heat fluxes considered.

t/t_c	Dimensionless surface temperature ($\Delta T_s/\Delta T_c$)				
	No loss	25	50	75	100
0.00	0.000	0.000	0.000	0.000	0.000
0.05	0.252	0.232	0.237	0.239	0.241
0.10	0.357	0.314	0.324	0.329	0.332
0.15	0.437	0.368	0.385	0.391	0.396
0.20	0.505	0.414	0.433	0.441	0.446
0.25	0.563	0.451	0.471	0.480	0.486
0.30	0.617	0.482	0.503	0.514	0.521
0.35	0.667	0.509	0.532	0.544	0.551
0.40	0.713	0.533	0.556	0.569	0.576
0.45	0.756	0.553	0.578	0.590	0.599
0.50	0.797	0.572	0.597	0.610	0.618
0.55	0.836	0.588	0.614	0.627	0.636
0.60	0.874	0.603	0.630	0.643	0.652
0.65	0.910	0.617	0.644	0.658	0.666
0.70	0.944	0.629	0.657	0.670	0.679
0.75	0.977	0.641	0.669	0.682	0.691
0.80	0.997	0.647	0.675	0.689	0.697

It should be pointed out that Tables 4 and 5 as well as Figure 6 strictly apply only for the assumptions that have been made regarding surface emissivity, convective heat transfer coefficient and ambient temperature. While these are expected to be reasonably appropriate for many applications, significantly different boundary conditions would require construction of one or more new set of tables and figures based on numerical calculations with the different boundary conditions.

The thermal inertia ratios shown in Figure 6 illustrate that as the nondimensional ignition time approaches a value of zero, i.e., for very high heat fluxes, the thermal inertia ratio approaches unity, as expected. Figure 6 also illustrates how the thermal inertia ratio decreases relatively rapidly as the ignition time moves away from the origin, with the slope decreasing with increasing time. From a practical standpoint, much of the ignition data reported in the literature is acquired for ignition times between about 0.25 and 1.0 characteristic times. Over this range, the thermal inertia ratio varies from approximately 0.75 down to approximately 0.37, suggesting that reported effective thermal inertias are approximately a factor of 1.3 to 2.7 times higher than the actual values would be.

Table 5. Ratio between numerical and no-loss surface temperatures (Surface temperature ratio) and between actual and effective thermal inertia (Thermal inertia ratio) as a function of dimensionless time.

	Incident heat flux (kW/m ²)				Incident heat flux (kW/m ²)			
	25	50	75	100	25	50	75	100
t/t _c	Surface temperature ratio				Thermal inertia ratio			
0.000	1.000	1.000	1.000	1.000	1.000	1.000	1.000	1.000
0.050	0.918	0.939	0.949	0.955	0.842	0.881	0.900	0.913
0.100	0.881	0.908	0.921	0.930	0.776	0.824	0.849	0.865
0.150	0.851	0.882	0.895	0.907	0.725	0.778	0.801	0.822
0.200	0.826	0.858	0.873	0.883	0.683	0.736	0.763	0.780
0.250	0.804	0.837	0.853	0.863	0.646	0.700	0.727	0.745
0.300	0.781	0.815	0.833	0.844	0.610	0.665	0.695	0.712
0.350	0.763	0.797	0.815	0.826	0.583	0.636	0.664	0.682
0.400	0.747	0.780	0.798	0.808	0.558	0.609	0.636	0.653
0.450	0.731	0.764	0.780	0.791	0.535	0.584	0.609	0.626
0.500	0.717	0.749	0.765	0.776	0.514	0.561	0.585	0.602
0.550	0.703	0.735	0.750	0.760	0.495	0.540	0.563	0.578
0.600	0.690	0.721	0.736	0.746	0.477	0.520	0.542	0.556
0.650	0.678	0.708	0.723	0.732	0.460	0.501	0.523	0.536
0.700	0.667	0.696	0.710	0.719	0.445	0.484	0.504	0.517
0.750	0.656	0.684	0.698	0.707	0.430	0.468	0.487	0.500
0.800	0.645	0.673	0.687	0.695	0.417	0.453	0.471	0.483
0.850	0.636	0.662	0.676	0.684	0.404	0.439	0.456	0.467
0.900	0.626	0.652	0.665	0.673	0.392	0.425	0.442	0.453
0.950	0.617	0.643	0.655	0.663	0.381	0.413	0.429	0.439
1.000	0.609	0.633	0.645	0.653	0.370	0.401	0.416	0.426

As an example application of this concept, consider a material with an ignition temperature of 350°C that ignites in 30 seconds when exposed to an incident heat flux of 50 kW/m². In accordance with the dimensional form of Equation 4, the effective thermal inertia of this material would be calculated as:

$$(k\rho c)_{eff} = \frac{4}{\pi} \left[\frac{\alpha \dot{q}_i''}{\Delta T_{ig}} \right]^2 t_{ig} = \frac{4}{\pi} \left[\frac{50}{330} \right]^2 30 = 0.877 \text{ (kW/m}^2\text{.K)}^2\text{.s} \quad (8)$$

Since the temperature ratios in Equation 7 depend on the characteristic time at ignition and the characteristic time is a function of the actual thermal inertia being sought, an iterative process is needed to solve for the actual thermal inertia. The actual thermal inertia will be some fraction of the effective thermal inertia. As a first approximation, assume the actual thermal inertia is 50 percent of the effective value. Then the characteristic time associated with this thermal inertia is

calculated, using the total heat transfer coefficient associated with this heat flux from Table 2, to be:

$$t_c = \frac{k\rho c}{h_{t,\max}^2} = \frac{0.877/2}{(0.079)^2} = 70.25 \text{ s} \quad (9)$$

With this value for t_c , the nondimensional ignition time becomes $t_{ig}/t_c = 30/70.25 = 0.427$. For this value of the dimensionless time, the surface temperature ratio is 0.772 and the thermal inertia ratio is 0.595 from Table 5. Since this thermal inertia value is significantly different from the assumed value of 0.50, further iteration is necessary.

As a second iteration, assume the thermal inertia ratio is 0.65. Then the characteristic time becomes 91.3 s and the nondimensional ignition time becomes 0.328. For this value of the nondimensional time, the surface temperature ratio is 0.805 and the thermal inertia ratio is 0.648 from Table 5, the same as the assumed value. Therefore, the actual thermal inertia would be $0.570 \text{ (kW/m}^2 \cdot \text{K)}^2 \cdot \text{s}$ rather than the effective value of $0.877 \text{ (kW/m}^2 \cdot \text{K)}^2 \cdot \text{s}$. For this same example, the Tewarson adjustment factor would have a value of 0.738, based on critical and incident heat fluxes of 13.1 and 50 kW/m^2 , respectively. This is 14 percent higher than the adjustment factor determined here.

As a check on these example calculations, the effective thermal inertia and the actual thermal inertia were used in the numerical calculations with an incident heat flux of 50 kW/m^2 . When the effective thermal inertia was used, an ignition time of 46.4 s was calculated; this value is 1.55 times greater than the actual ignition time of 30 seconds, which is very close to the inverse of the thermal inertia ratio ($1/0.65$), as would be expected. When the actual thermal inertia was used, an ignition time of 30.5 s was calculated; the small difference of 0.5 s is most likely due to rounding errors. Based on the thermal inertia associated with the Tewarson adjustment factor, the calculated ignition time would be 34.3 s, a value 14 percent higher than the actual ignition time, which would be expected based on the ratio between the two adjustment factors (i.e., $0.738/0.65 = 1.14$). This ratio between the adjustment factors can also be used to evaluate actual thermal inertias from effective thermal inertias determined with Equation 5, i.e., the Tewarson solution.

Further discussion

The analysis presented in this paper indicates that actual thermal inertias can be significantly lower than effective thermal inertias determined on the basis of Equation 4 and as indicated in Figure 6. This will depend to a large extent on the heat fluxes at which the effective thermal inertias have been determined, with the effect being smaller at higher heat fluxes. While the effective values reported in the literature are still of great use for ignition and flame spread models based on similar assumptions, i.e., no surface heat losses, and for ranking materials in terms of relative values, these effective values will underestimate the potential for ignition and flame spread when used with models that calculate heat losses directly based on convective-radiative boundary conditions.

The method presented here for determining actual thermal inertias based on effective thermal inertias available in the literature can also be used to evaluate new ignition test data. One aspect of interpreting both existing and new data sets that needs to be explored is how this method will be applied to data acquired over a wide range of heat fluxes. The standard procedure for determining effective thermal inertia values is to plot $t_{ig}^{-1/2}$ versus $\alpha \dot{q}_i''$, with the effective thermal inertia related to the slope of the best fit line through the data. This suggests that either no adjustment factor or a constant adjustment factor applies equally well to all the data points. This is inconsistent with the analysis presented here, which suggests that the adjustment factor will vary with the incident heat flux, with a larger adjustment factor associated with ignition data acquired at lower heat fluxes. Future work will include the analysis of some existing data sets to evaluate this issue.

It should be recognized that there are limitations associated with the approach presented here, whether applied to new or existing data. To a large extent, these are the same limitations that have always been associated with the methods used to determine effective thermal properties from small-scale radiant exposure experiments. The actual thermal inertias discussed in this paper are still temperature-independent average values. The temperature dependence of these properties and the effects of moisture content and other latent heat effects have not been addressed. This analysis has also assumed that the concept of an inert solid with a distinct and constant ignition temperature is valid. As more sophisticated models of fire spread are developed and implemented, there is a need to develop more precise properties that explicitly account for temperature-dependence, latent heat effects, variable ignition temperatures and ignition delay times in order to more accurately calculate ignition, flame spread and other reaction-to-fire phenomena for solid materials.

Summary and conclusions

Methods for deriving effective thermal inertia values for thermally thick materials based on small-scale radiant exposure tests have been reviewed and analyzed. None of these methods accurately captures the surface temperature history of thermally thick solids subjected to constant incident heat fluxes, primarily because they either ignore surface heat losses entirely or treat them in a way that does not accurately account for the highly nonlinear dependence of surface reradiation on the surface temperature. This is demonstrated by the comparisons with numerical results that have been presented in this paper.

The numerical results were calculated using an explicit finite difference scheme for a range of incident heat fluxes from 25 to 100 kW/m² and a range of thermal inertias from 0.001 to 1 (kW/m².K)².s. These ranges are fairly representative of the exposure conditions and building materials commonly used. The numerical calculations were nondimensionalized in terms of characteristic times and temperatures, with the outcome that the temperature curves converged to a relatively small range of results for the range of heat fluxes and thermal inertias considered.

Differences between effective and actual thermal inertia values were analyzed, with the effective thermal inertia found to be approximately a factor of 1.33 to 2.75 greater than the actual value over a representative range of characteristic times, although this factor will depend on a number

of factors that have not been fully explored here. A methodology was developed to determine actual thermal inertia values from effective values. This methodology has value for translation of the large body of effective thermal property data currently available in the literature as well as for the analysis of future ignition data. While the published effective property data will continue to be useful for calculations based on similar assumptions, the more accurate actual thermal inertia values are needed for more detailed calculations, such as those included in the current version of the FDS model [11].

Finally, it should be recognized that the analysis presented here is based on the same thermal arguments used for the determination of effective properties and does not address additional issues related to the determination of more precise material flammability properties. These issues have been identified and are associated with the generation of sufficient fuel for sustained ignition, in-depth generation of fuel, pilot location, and other factors [1, 12].

Acknowledgements

This work was supported by the Building and Fire Research Laboratory of the National Institute of Standards and Technology, with Mr. Daniel Madrzykowski serving as the technical advisor. This support is gratefully acknowledged.

References

1. Drysdale, D., *An Introduction to Fire Dynamics*, 2nd Edition, John Wiley & Sons, Chichester, 1999.
2. Kreith, F., *Principles of Heat Transfer*, 3rd Edition, Harper & Row, New York, 1973.
3. ASTM E1321, *Standard Test Method for Determining Material Ignition and Flame Spread Properties*, ASTM International, West Conshohocken, PA, 2000.
4. ASTM E1354, *Standard Test Method for Heat and Visible Smoke Release Rates for Materials and Products Using an Oxygen Consumption Calorimeter*, ASTM International, West Conshohocken, PA, 2000.
5. ASTM E2058, *Standard Test Methods for Measurement of Synthetic Polymer Material Flammability Using a Fire Propagation Apparatus (FPA)*, ASTM International, West Conshohocken, PA, 2002.
6. Steinhaus, T., Masters Thesis, Department of Fire Protection Engineering, University of Maryland, College Park, 1999.
7. Cordova, J.L., Walther, D.C., Torero, J.L. and Fernandez-Pello, A.C., "Oxidizer Flow Effects on the Flammability of Solid Combustibles," *Combustion Science and Technology*, v. 164, No-1-6, pp. 253-278, 2001.
8. Long, R.T., Jr., Torero, J.L., Quintiere, J.G., and Fernandez-Pello, A.C., "Scale and Transport Considerations on Piloted Ignition of PMMA," *Fire Safety Science – Proceedings of the 6th International Symposium*, International Association for Fire Safety Science, 2000.
9. Hurley, M.J., and Quiter, J.R., "Simple Fire Hazard Calculations," Section 3/Chapter 10, *Fire Protection Handbook*, 19th Edition, National Fire Protection Association, Quincy, MA, 2003.

10. Tewarson, A., "Generation of Heat and Chemical Compounds in Fires," Chapter 4/Section 3, *SFPE Handbook of Fire Protection Engineering*, 3rd Edition, National Fire Protection Association, Quincy, MA, 2002. Tewarson
11. McGrattan, K. B., H.R. Baum, R.G. Rehm, A. Hamins, G.P. Forney, J.E. Floyd, S. Hostikka, and Prasad, K., Fire Dynamics Simulator (Version 3) – Technical Reference Guide, *NISTIR 6783*, National Institute of Standards and Technology, Gaithersburg, MD, November 2002.
12. Torero, J.L., and Mowrer, F.W., "A New Approach to Interpreting LIFT Ignition Test Data," *Proceedings of the Thirty-First International Conference on Fire Safety*, Product Safety Corporation, Columbus, OH, July 2000.

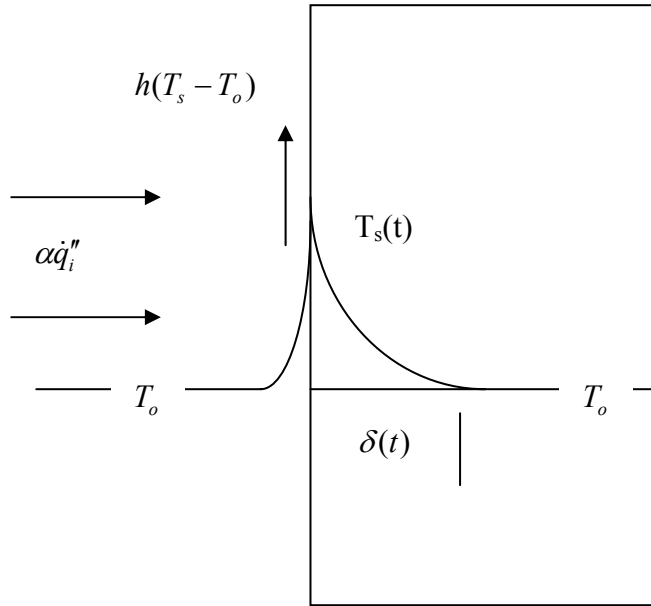


Figure 1. Schematic diagram of thermally thick heating scenario.

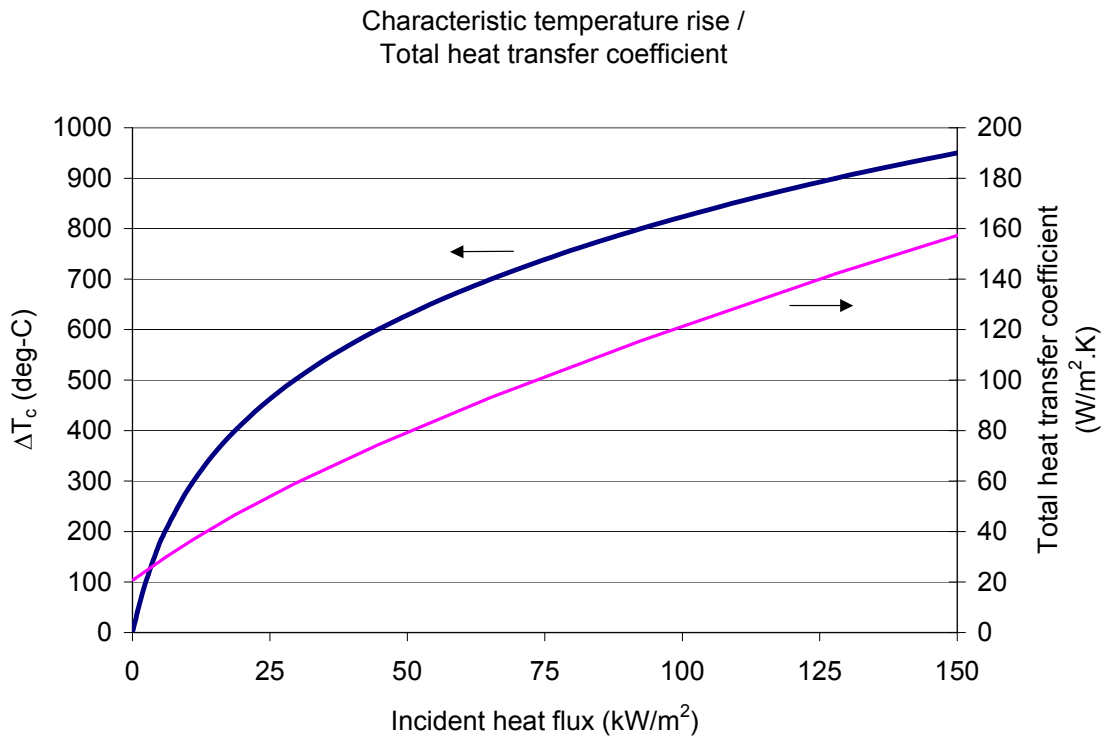


Figure 2. Characteristic temperature rise and total heat transfer coefficient as a function of incident heat flux.

Analytical and numerical solutions
Incident heat flux = 25 kW/m²

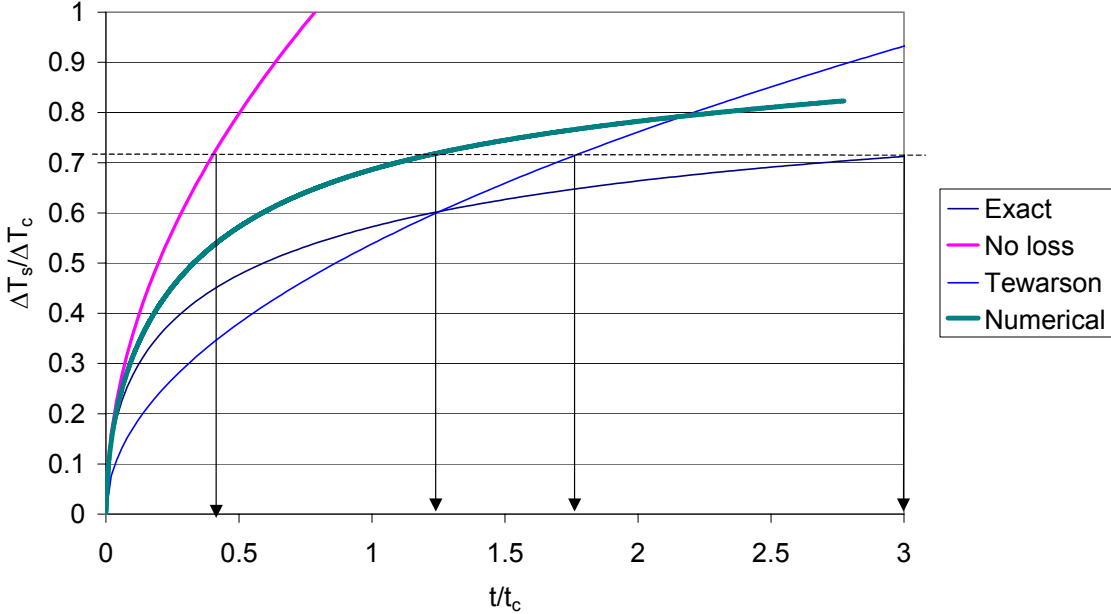


Figure 3(a). Comparison of analytical and numerical solutions for surface temperature and time to ignition at an incident heat flux of 25 kW/m².

Analytical and numerical solutions
Incident heat flux = 50 kW/m²

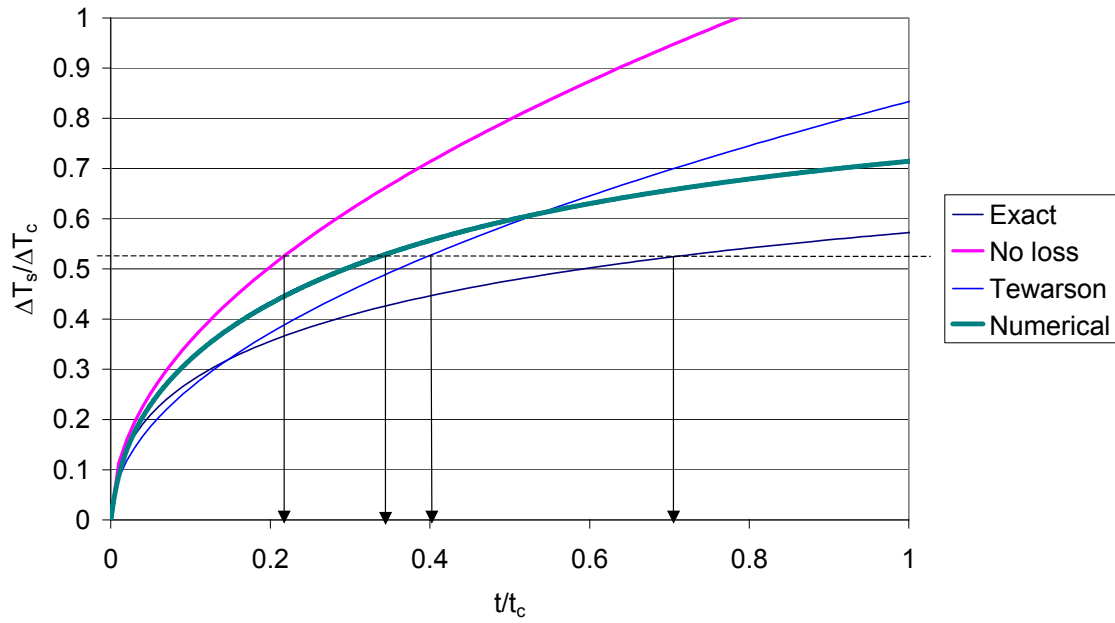


Figure 3(b). Comparison of analytical and numerical solutions for surface temperature and time to ignition at an incident heat flux of 50 kW/m².

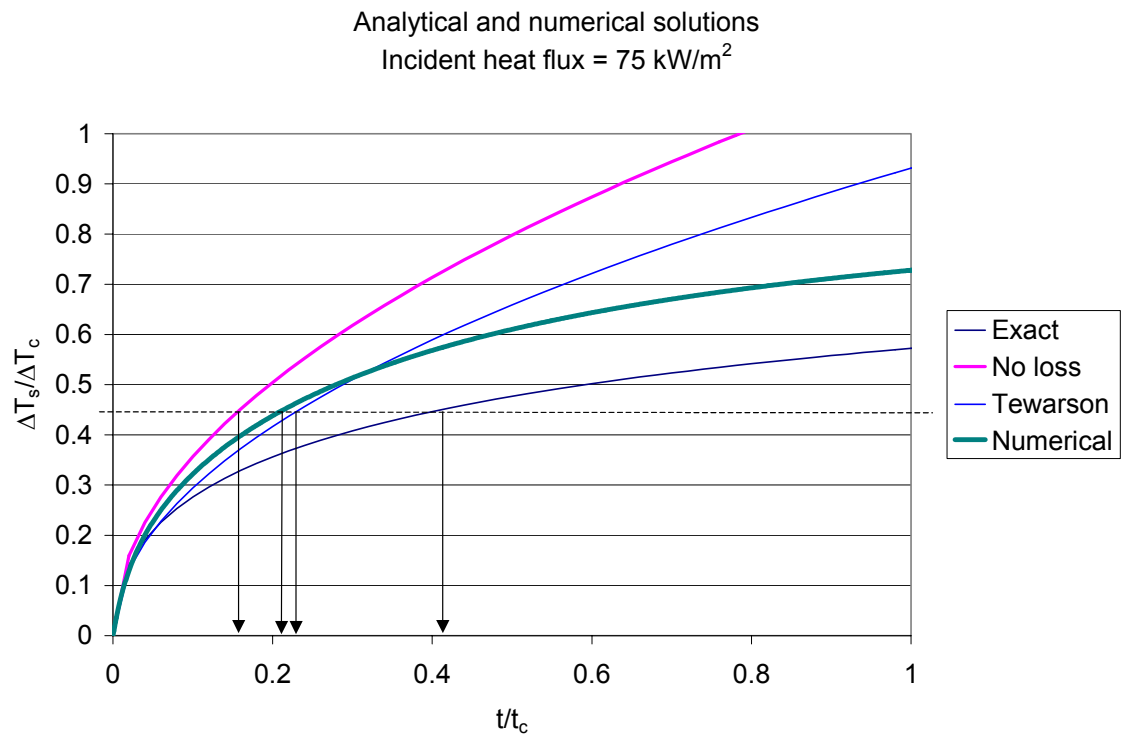


Figure 3(c). Comparison of analytical and numerical solutions for surface temperature and time to ignition at an incident heat flux of 75 kW/m².

Analytical and numerical solutions
Incident heat flux = 100 kW/m²

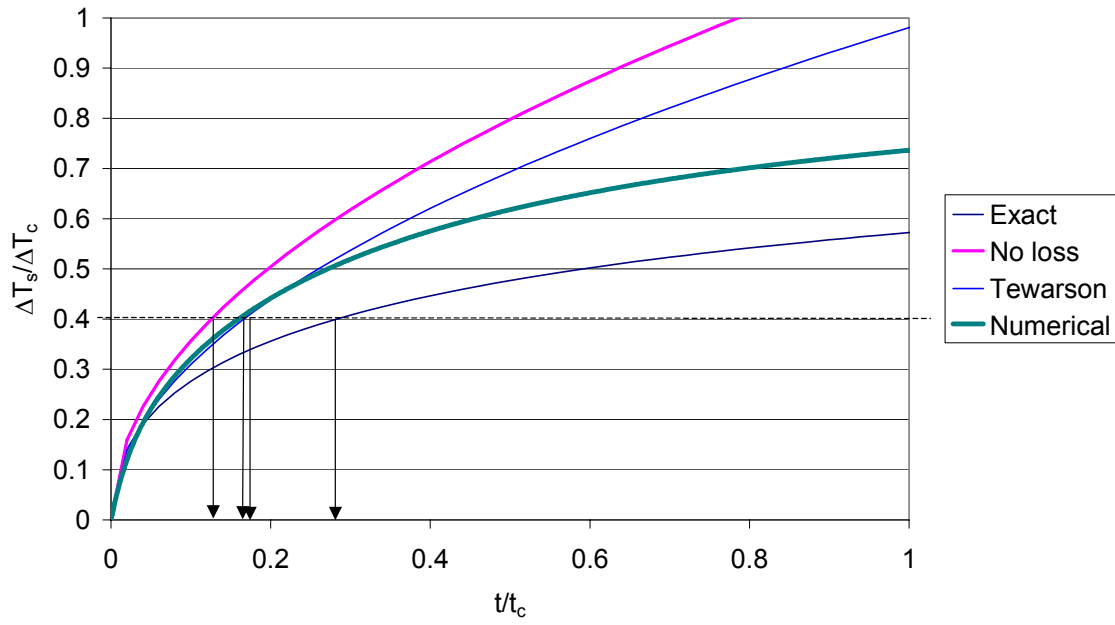


Figure 3(d). Comparison of analytical and numerical solutions for surface temperature and time to ignition at an incident heat flux of 100 kW/m².

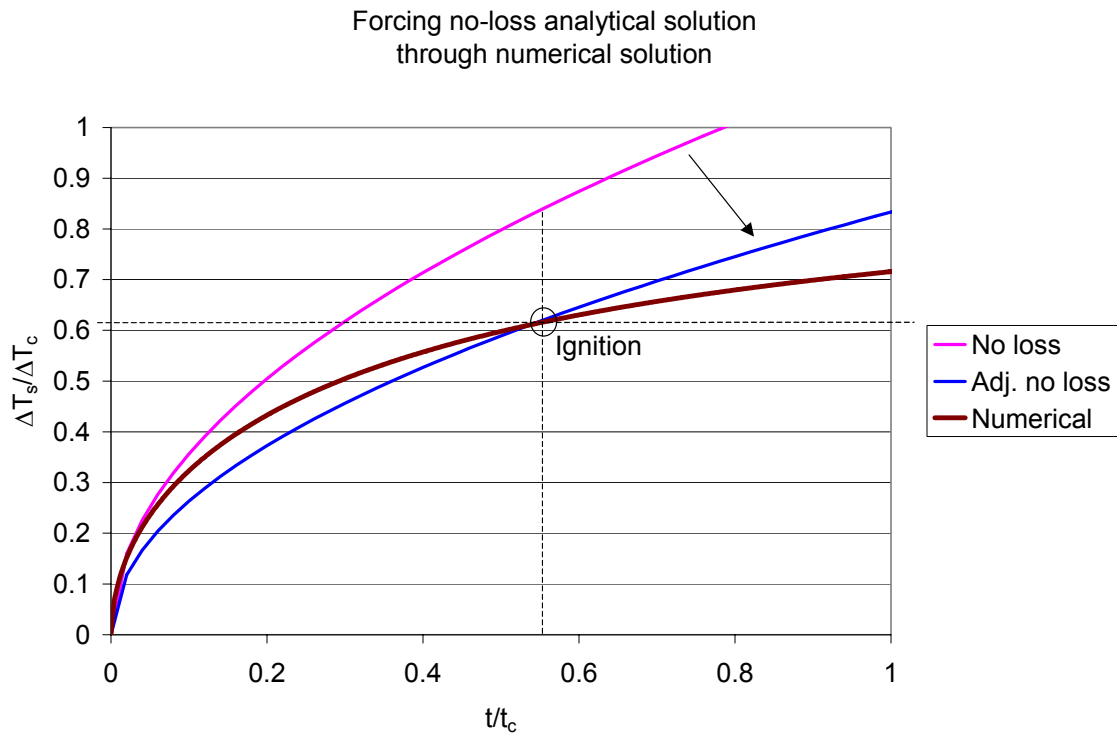


Figure 4. Illustration of method for adjusting the no-loss analytical solution through the ignition point.

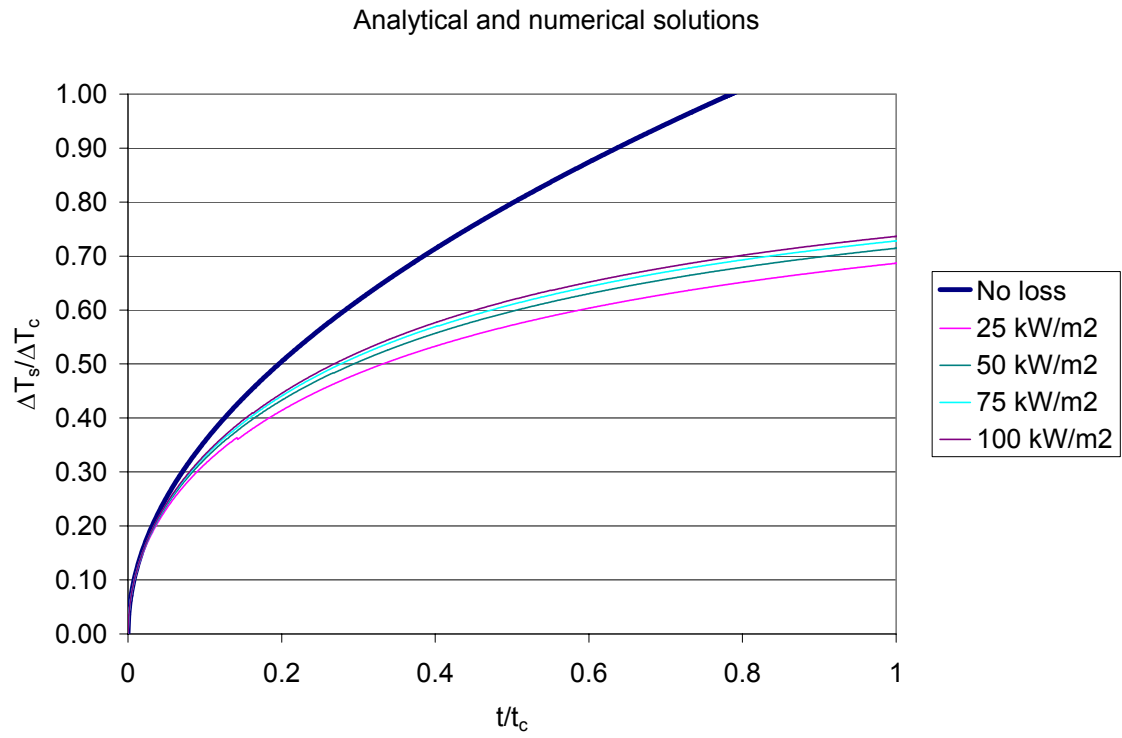


Figure 5. Comparison of analytical solution based on no heat losses (Equation 4) with numerical results for range of incident heat fluxes.

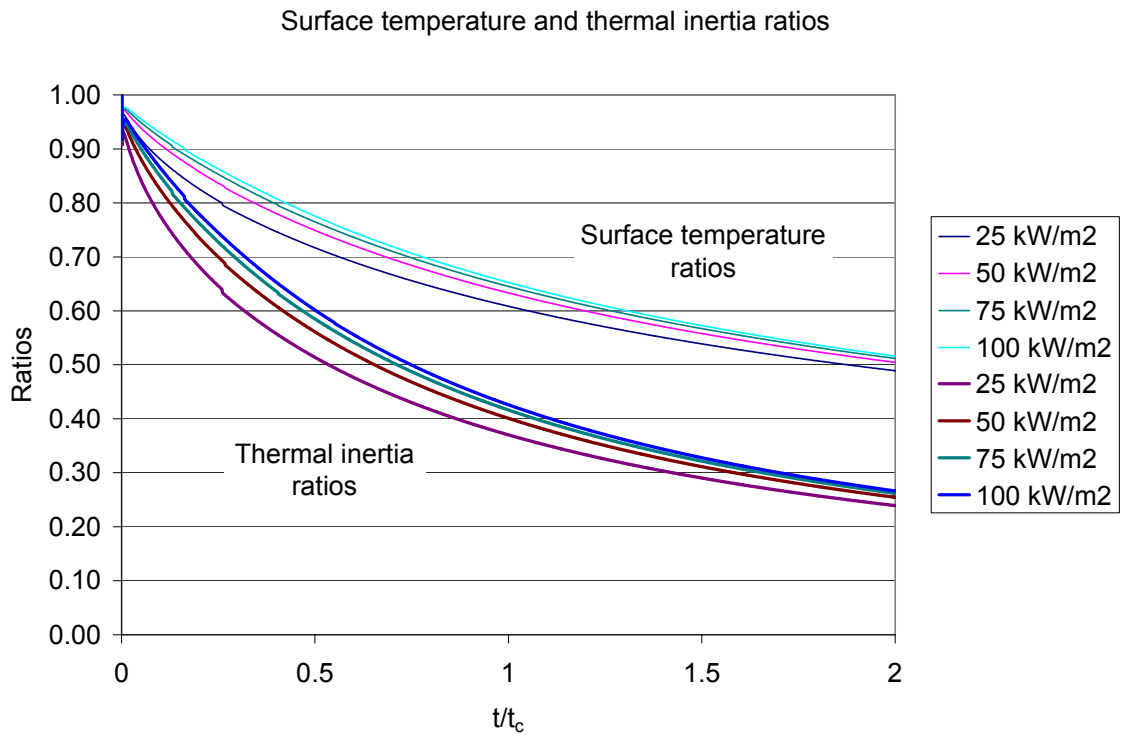


Figure 6. Ratio between the surface temperatures determined numerically and for the no-loss analytical solution and between the actual and effective thermal inertias based on Equation 6 and the surface temperature ratios.